Pergamon

*Int. J. Heat Mass Transfer.* Vol. 37, No. 3, pp. 443–450, 1994

0017–9310/94 $6.00 + 0.00

# Complementary upper and lower truncated sum, multiple scattering bounds on the effective emissivity

YONG XIA and WILLIAM STRIEDER†
Department of Chemical Engineering, University of Notre Dame, Notre Dame, IN 46556, U.S.A.

(*Received* 8 *December* 1992 *and in final form* 19 *July* 1993)

**Abstract**—Two different infinite series in one minus the surface emissivity $(1-\varepsilon_s)^i$ are developed for the effective emissivity $\varepsilon_{eff}$ of an isothermal semi-infinite slab with an arbitrary void–solid distribution. The coefficients for the $i$th term of each series depend on a single set of $i$ integrals $H_0, H_1, \ldots, H_i$ where $H_i$ counts the escape path probabilities of an emitted photon with exactly $i$ surface reflections. Rigorous complementary upper and lower bounds on $\varepsilon_{eff}$ and useful estimates with error bounds can be generated after evaluating just the first few $i$ terms of each series. Explicit calculations are given for a model random void–solid distribution, a semi-infinite slab cut from a bed of randomly overlapping spheres, and to the level $H_0$, $H_1$ provide good estimates of $\varepsilon_{eff}$ for $\varepsilon_s > 0.6$ for any void fraction. Results are compared to two-flux and cell model calculations as well as available experimental data.

## INTRODUCTION

RADIATION heat transport from a randomly distributed solid is generally important at higher temperatures. For example radiative losses from the external surfaces of porous solid reactants [1] play an important role in the high temperature combustion wave synthesis of advanced ceramic materials. The external circumference of the cylindrical pellets used to make silicon nitride may reach 4000°C as the reaction wave passes. On the other hand, to sustain non-catalytic gas–solid reactions such as the reduction of ores or the roasting of sulfides requires radiant heat transport to the outside surface of the porous reacted shell [2]. The contribution of radiative heat flux both from the bubble and the emulsion phases must be included in the total heat transfer from gas fluidized beds. Saxena *et al.* [3] have pointed out, in their review of experimental techniques for the measurement of radiative and total heat transfer from high temperature gas fluidized beds, that appreciable differences exist in measured quantities, e.g. the ratio of radiant to total energy flux from the fluidized bed, whenever a comparison between literature or experimental sources is possible. A model for the heat transport processes for any of these systems will require an effective surface emissivity $\varepsilon_{eff}$ for the porous solid, or for the fluidized bed emulsion phase, to properly include radiant transport to, or from, the surroundings.

In earlier work Brewster [4, 5] derived an expression for the effective bed emissivity of an isothermal fluidized bed. The radiative transport within the dispersion was represented by the two-flux model. Tien and Drolen [6] have pointed out that the two-flux model can be inaccurate in any bed of anisotropically scattering particles. In addition the bed adsorption and scattering coefficients used by Brewster [5] limit the application to dilute particle beds.

Borodulya *et al.* [7, 8] in their calculation of $\varepsilon_{eff}$ for an isothermal bed have explicitly included the bed structure as a stationary cubic lattice arrangement of solid spherical particles. In order to treat a single unit cell of the lattice as a closed system, the cell faces that cut the void space were assumed to be black, diffusive planar surfaces, and approximate network theory [9] was used. Vortmeyer [10] has pointed out, in his review of radiation transport models in packed solids, that as a result of these approximations cell models do not include long range scattering in a rigorous manner. Borodulya *et al.* [7] generated numerical values for the effective bed emissivity of both a packed and an expanded lattice of spheres, as a function of the particle emissivity.

In addition, Grace [11] has proposed an empirical relationship between the effective emissivity of a fluidized bed and the particle emissivity. One difficulty common to all these previous efforts is the failure to obtain a clear, systematic relationship between the effective emissivity and bed structure.

For high temperature transport processes within porous solids, there are numerous instances [1, 2, 12] where the temperature gradients normal to the porous solid external surface can be neglected, and the surface radiation term is either locally isothermal in the differential element or is globally isothermal. In the second case of a high temperature fluidized bed, due

† Author to whom correspondence should be addressed.

## NOMENCLATURE

$G_i$, $H_i$ $i$th coefficient of $\varepsilon_{\text{eff}}$ in upper (14) and lower (15) bound sums
$K(r', r)\,d^2r$ local differential view factor between a unit surface at $r'$ and $d^2r$
$Q(x, y)$ integral defined in (29b) and (29c)
$T$ temperature
$a$ the radius of randomly distributed spheres
$d^2r^{(i)}$ element of surface area located at $r^{(i)}$ on either $\Sigma_s$ or $\Sigma_0$
$m$ average pore diameter
$v_1$ the two-step path exclusion volume.

Greek symbols
$\beta$ the density of sphere centers
$\varepsilon$ emissivity
$\eta(r)$ unit normal vector at void–solid interface position $r$ into the void
$\rho, \rho'$ the displacement vector, defined as $(r'-r)$ and $(r''-r')$
$d^3\rho$ slab volume integral element
$d^2\rho'$ surface area integral element on $\Sigma_0$
$\sigma_s$ total sphere area, overlapped or not, per unit total volume
$\Sigma_0$ an infinite surface area next to the slab boundary $x = 0$
$\Sigma_s$ void–solid interface surface area
$\phi$ void fraction.

Subscripts and others
eff effective
ext void–solid interface at slab boundary $x = 0$
int void–solid internal interface
$\langle\ \rangle_1$ mid point estimates.

to the high degree of solid particle mixing, an isothermal bed is often a reasonable first approximation. Indeed, for large particle fluidized beds (diameter $>1$ mm), isothermal conditions are an accurate assumption [11, 13, 14]. In this paper expressions for the effective emissivity are developed for a void–solid system of arbitrary geometry and a uniform temperature $T_s$.

We will consider the characteristic diameter of the solid particles used to construct the void–solid distribution as sufficiently larger than the wavelength of the thermal radiation [9], and the characteristic distance between neighboring solid particles as small enough [7, 8], that the radiative transfer may be regarded as occurring due to multiple optical reflections at the void–solid interface. The solid is opaque with gray emitting–diffusely reflecting surfaces, a local surface emissivity $\varepsilon_s$, and Kirchoff's law assumed [9]. The void gas is taken to be transparent.

In the next section, two different analytical cum simulation expansions for the effective emissivity of a semi-infinite bed of arbitrary void–solid geometry are derived. When both summation expressions are truncated at the same order in the expansion variable $(1-\varepsilon_s)$, complementary upper and lower bounds on $\varepsilon_{\text{eff}}$ are generated. Explicit, analytical upper and lower bounds on $\varepsilon_{\text{eff}}$ are calculated in Section 3, for a thick bed generated by slicing an infinite plane through a bed of randomly placed, freely overlapping solid spheres all of the same radius (Fig. 1(a)).

## FORMULATION OF EQUATIONS

The effective emissivity is a thermodynamic coefficient that measures the ability of a random surface to emit or absorb radiation. In order to evaluate $\varepsilon_{\text{eff}}$, transport equations must be formulated based on the microstructure of the void–solid bed. Suppose just outside the edge at $x = 0$ of a semi-infinite bed (Fig. 1(a)), a plane $\Sigma_0$ is positioned, and that $i$ is a unit vector in the positive $x$-direction. The bed is divided into arbitrary solid and void regions. The void–solid interface $\Sigma_s$, between these two regions, includes the solid surface at $x = 0$.

As we assume $\Sigma_s$ is an opaque gray diffuse surface, the radiation is emitted and reflected diffusely according to Lambert's cosine law [9]. The emitted radiative flux from a unit element of $\Sigma_s$ depends on the absolute temperature $T_s$ of the surface, the surface emissivity $\varepsilon_s$ and the Stefan–Boltzmann constant $\sigma$, in the combination $\varepsilon_s\sigma T_s^4$. Kirchhoff's law states that the same surface element will absorb only a fraction $\varepsilon_s$ of the incident radiation, reflecting the portion $(1-\varepsilon_s)$.

The fraction $K(r', r)d^2r$ of the total radiation from a unit surface element located at $r'$ on $\Sigma_s$, that travels

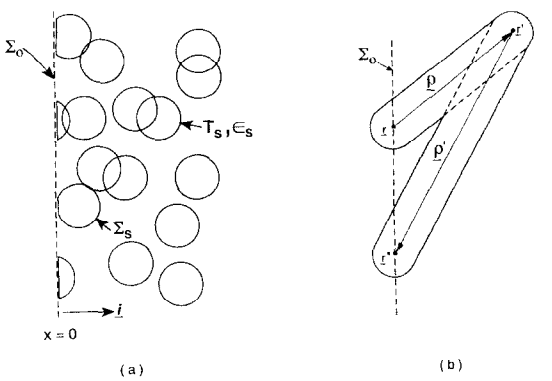


FIG. 1. (a) Edge of a semi-infinite bed of overlapping spheres; (b) exclusion volume $v_1$ for a two-step path.

a straight line free path, and arrives at a second surface element $d^2r$ located at $r$ on $\Sigma_s$, can be used to formulate the radiant exchange between surfaces. Note the function $K(r', r)$ is also defined when $r'$ is located at the void–solid interface $\Sigma_s$, but $r$ lies on the plane surface $\Sigma_0$. Since we are assuming diffuse scattering and emission from the void–solid interface, $K(r', r)$ is given by the cosine law

$$K(r', r) = K(r, r'), \tag{1}$$

$$= -[\eta(r)\cdot\rho][\eta(r')\cdot\rho]/(\pi\rho^4) \quad (\text{if } r' \text{ can see } r), \tag{2a}$$

$$= 0 \quad (\text{otherwise}), \tag{2b}$$

where $\eta(r)$ and $\eta(r')$ are unit normals, respectively, at $r$ and $r'$ pointing into the void on $\Sigma_s$ or pointing in the $i$ direction on $\Sigma_0$, and $\rho = (r'-r)$.

The portion of the radiation emitted by the bed surface $\Sigma_s$, that finds its way across the plane $\Sigma_0$ before reabsorption, can be regarded as the sum of contributions from all possible paths of photons, that begin with emission from a differential element on $\Sigma_s$, travel a zig-zag path of successive diffuse reflections and leave the bed across $\Sigma_0$. These possible paths can be denumerated by the number $i$ of internal void–solid interface diffuse reflections the emitted photon makes before exiting. Of the photons emitted from any surface element $d^2r^{(i+1)}$ at $r^{(i+1)}$ on $\Sigma_s$, the fraction $K(r^{(i+1)}, r^{(i)})\, d^2r^{(i)}$ will travel directly to $r^{(i)}$ and collide within $d^2r^{(i)}$. Of these the portion $(1-\varepsilon_s)$ will be reflected from $d^2r^{(i)}$ and, as the reflection is diffuse, the fraction $K(r^{(i)}, r^{(i-1)})\, d^2r^{(i-1)}$ of these reflected photons will arrive at $r^{(i-1)}$ and collide within $d^2r^{(i-1)}$ and so forth. The photons emitted from $d^2r^{(i+1)}$, that make $i$ successive diffusive reflections from the surface elements $d^2r^{(i)}, d^2r^{(i-1)}, \ldots, d^2r'$ on $\Sigma_s$, and travel out of the bed across a surface element $d^2r$ on $\Sigma_0$, make a contribution to the total radiation emitted from the bed per unit area $\Sigma_0$ of

$$(1-\varepsilon_s)^i H_i \varepsilon_s \sigma T_s^4 \equiv (1-\varepsilon_s)^i \Sigma_0^{-1} \int_{\Sigma_0} d^2r \times \int_{\Sigma_s} d^2r' \ldots \int_{\Sigma_s} d^2r^{(i+1)} K(r', r)K(r'', r') \ldots K(r^{(i+1)}, r^{(i)})\varepsilon_s \sigma T_s^4, \tag{3}$$

where the integrations sum over all possible paths with $i$ diffuse reflections that start with emission at any $r^{(i+1)}$ on $\Sigma_s$ and end at any $r$ on $\Sigma_0$. Then the total radiation emitted from the bed across $\Sigma_0$ per unit area

$$\varepsilon_{\text{eff}} \sigma T_s^4 = \sum_{i=0}^{\infty} (1-\varepsilon_s)^i H_i \varepsilon_s \sigma T_s^4 \tag{4}$$

provides an expression for the effective emissivity.

From the expression (4) with the definition (3) of $H_i$, the first summation form for the effective emissivity is

$$\varepsilon_{\text{eff}} = \sum_{i=0}^{\infty} (1-\varepsilon_s)^i \varepsilon_s H_i, \tag{5}$$

where

$$H_i \equiv \Sigma_0^{-1} \int_{\Sigma_0} d^2r \int_{\Sigma_s} d^2r' \ldots \int_{\Sigma_s} d^2r^{(i+1)} K(r', r) \times K(r'', r') \ldots K(r^{(i+1)}, r^{(i)}). \tag{6}$$

Since $K(r', r)\, d^2r$ is a positive fraction, less than unity, and all possible straight line path segments from $r'$ on $\Sigma_s$ will end in either $\Sigma_s$ or $\Sigma_0$, we have

$$\int_{\Sigma_s} K(r', r)\, d^2r + \int_{\Sigma_0} K(r', r)\, d^2r = 1 \quad (r \text{ on } \Sigma_s). \tag{7}$$

From these considerations along with (5) and (6), the following properties for $H_i$ are obtained:

$$0 \leqslant H_i \leqslant 1, \quad i = 0, 1, \ldots, \infty, \tag{8}$$

$$H_i \leqslant H_{i-1}, \quad i = 0, 1, \ldots, \infty, \tag{9}$$

$$H_0 = 1, \tag{10}$$

and $H_i$ depends only on the structural properties of the void–solid distribution. Note that the inequalities (8) and (9) imply the convergence of the series (5). As every term in (5) is positive, any truncation of this series gives a lower bound on $\varepsilon_{\text{eff}}$. Hence $\varepsilon_s$ is always a zeroth order lower bound on $\varepsilon_{\text{eff}}$ for any solid structure, and including the $H_0$ and $H_1$ terms in (5), we have the improved first order lower bound

$$\varepsilon_{\text{eff}} \geqslant \varepsilon_s + (1-\varepsilon_s)\varepsilon_s H_1. \tag{11}$$

A second complementary summation form can be obtained by defining $G_i$

$$G_i = \Sigma_0^{-1} \int_{\Sigma_0} d^2r \int_{\Sigma_s} d^2r' \ldots \int_{\Sigma_s} d^2r^{(i)} \times \int_{\Sigma_0} d^2r^{(i+1)} K(r', r)K(r'', r') \ldots K(r^{(i+1)}, r^{(i)}) \quad i = 1, 2, \ldots, \infty, \tag{12}$$

and noting from (6) and (7) that

$$G_i = H_{i-1} - H_i, \quad i = 1, 2, \ldots, \infty. \tag{13}$$

With (13), the summation (5) for the effective emissivity can be recast in a second form,

$$\varepsilon_{\text{eff}} = H_0 - \sum_{i=1}^{\infty} (1-\varepsilon_s)^i G_i. \tag{14}$$

As $G_i$ from (12) and hence every term $(1-\varepsilon_s)^i G_i$ in the series (14) is positive, a truncation at any $i$ value gives an upper bound on $\varepsilon_{\text{eff}}$ reciprocal to (11). In the sense that the $i$th order upper and lower bounds depend on the same set of integrals $H_i, H_{i-1}, \ldots, H_0$ they are complementary. Hence unity is always a zeroth order upper bound for any solid semi-infinite structure, and taking only the $H_0$ and $G_1$ terms from (14) we have the improved first order upper bound

$$\varepsilon_{\text{eff}} \leqslant 1-(1-\varepsilon_s)(1-H_1). \tag{15}$$

Equations (10) and (13) permit both the reciprocal bounds (11) and (15) to be written in terms of the same path integral $H_1$. Values of $H_1$ can always be obtained by direct Monte Carlo computation of the paths, where only the lowest order two-segment free paths need be considered. For some structures analytical results are available and, to examine the method, analytical reciprocal upper and lower bounds on $\varepsilon_{\text{eff}}$ are calculated for a model random porous medium in the next section.

## BOUNDS ON $\varepsilon_{\text{eff}}$ FOR A MODEL RANDOM BED

One random geometry that permits an analytical formulation of the free paths is obtained when a single plane is sliced through an infinite bed of randomly placed, freely overlapping solid spheres all of the same radius (Fig. 1(a)). All those points within the slab lying on a sphere surface but not in the interior of one or more overlapping spheres, plus the slab edge surfaces generated when the solid spheres were cut, make up the void–solid interface $\Sigma_s$. The points within the interior of one or more spheres make up the solid. At intermediate void fractions the model porous solid appears as ductile spheres that have been compressed together under a deformation pressure, or instead a porous slab that has been cut from a larger sintered block. A bed of randomly overlapping spheres at higher sphere center densities (lower void fraction) has the required shape irregularities found in some porous solids, including surface crevices, branching and pore pinching. At lower densities (higher void fraction) the randomly placed spheres resemble a fluidized, dispersed solid bed.

The bed is produced by placing $N$ sphere centers, totally independently of each other [15], into a very large volume $V$. Solid spheres of radius $a$ are then placed around these centers, and allowed to overlap freely. The probability $P$ that a volume $v$ is free of sphere centers, after adding $N$ spheres into a large volume $V$, is

$$P = [(V-v)/V]^N. \tag{16}$$

Taking the limit of this expression as $N$ and $V$ become infinite, we have

$$P = \exp[-\beta v], \tag{17}$$

where the density of sphere centers is defined as $\beta(=N/V)$. The event that a point is in the void, requires sphere centers be excluded from a spherical volume of radius $a$ about the point, and the probability of finding a point in the void from (17) is

$$\phi = \exp[-4\pi a^3\beta/3]. \tag{18}$$

This quantity is also the void fraction or porosity $\phi$. The total sphere area $\sigma_s$, overlapped or not, per unit total volume is

$$\sigma_s = 4\pi a^2\beta, \tag{19a}$$

and from the porosity (18), the exposed (not overlapped) sphere surface area $s$ per unit total slab volume is

$$s = 4\pi a^2\beta\phi. \tag{19b}$$

The surface area given by (19) does not include the edge surfaces created when the spheres were cut, these must be considered separately. The average pore diameter $m$, often used in place of $s$, is defined as four times the void volume divided by the internal surface area

$$m = \frac{4\phi}{s} = (\pi a^2\beta)^{-1}. \tag{19c}$$

The reciprocal bounds (11) and (15) require the evaluation of either $H_1$ or $G_1$ which are related by (10) and (13)

$$H_1 = 1-G_1. \tag{20}$$

From (12), the $\Sigma_s$ integration of $G_1$ can be written as a sum of two terms, one that accounts for the cut area of the solid spheres $\Sigma_{\text{ext}}$ and a second that includes the internal void–solid interface area $\Sigma_{\text{int}}$ of the bed.

$$G_1 = \Sigma_0^{-1}\int_{\Sigma_0} d^2r \int_{\Sigma_{\text{ext}}} d^2r' \int_{\Sigma_0} d^2r'' K(r',r)K(r'',r')$$
$$+\Sigma_0^{-1}\int_{\Sigma_0} d^2r \int_{\Sigma_{\text{int}}} d^2r' \int_{\Sigma_0} d^2r'' K(r',r)K(r'',r'). \tag{21}$$

As all radiation that leaves the surface element $d^2r'$ on $\Sigma_{\text{ext}}$ must pass across $\Sigma_0$ both the integrals of $K$ over $\Sigma_0$ in the first term in (21) are unity. The area $\Sigma_{\text{ext}}$ is the solid area of a slab cross-section and

$$G_1 = 1-\phi+\Sigma_0^{-1}\int_{\Sigma_0} d^2r \int_{\Sigma_{\text{int}}} d^2r' \times \int_{\Sigma_0} d^2r'' K(r',r)K(r'',r') \tag{22}$$

where $\Sigma_{\text{int}}$ sums over the internal spherical surface elements of the semi-infinite slab.

From equations (2a) and (2b) for the jump probability $K(r', r)$, the integrand of (22) depends on the displacement vectors $\rho = r'-r$ and $\rho' = r''-r'$; the surface normal $\eta'$ located at $r'$ on $\Sigma_{\text{int}}$; and the free path event that the surface point $r'$ can see both $r$ and $r''$ on $\Sigma_0$. For a fixed $\rho$, $\rho'$, $d^2r$ and $d^2r''$, if $d^3\rho$ is an element of volume in the slab at the tip of $\rho$, then $\sigma_s d^3\rho\, d^2\eta'/(4\pi)$ is the internal area, overlapped or not, in $d^3\rho$ with surface unit normal $\eta'$ lying in the solid angle element $d^2\eta'$. The operation

$$\Sigma_0^{-1}\int_{\Sigma_0} d^2r$$

for a fixed $\rho$, $\rho'$ and $\eta'$ is an average over the entire plane $\Sigma_0$, and with the free path event of the integrand, it generates the probability that the points $r$ and $r''$ at

the edge of the slab are in the void, that the sphere surface point $r'$ is not overlapped by the other spheres of suspension, and that the two-segment free path from $r$ to $r'$ and $r'$ to $r''$ is free of obstructions. This event requires that sphere centers be excluded from right circular cylinders of radius $a$ about $\rho$ and $\rho'$, as well as spheres of radius $a$ about the base of $\rho$ and the tips of $\rho$ and $\rho'$ (Fig. 1(b)). Quite apart from the overlapping of the solid spheres, elements of the exclusion volume may overlap. Any overlapped volume is counted only once, the net exclusion volume (Fig. 1(b)) is denoted as $v_1$ and the free path event probability $P_1$ given by (17) is

$$P_1 = \exp[-\beta v_1]. \tag{23}$$

The vector $\rho$ runs from a point on the plane $\Sigma_0$ to all elements of volume $d^3\rho$ in the slab and the vector $\rho'$ runs from $d^3\rho$ to all elements of surface $d^2\rho'$ in the plane $\Sigma_0$. With these limits for the integral $G_1$ and using the excluded volume probability (23), we have

$$G_1 = 1-\phi+\sigma_s\int d^3\boldsymbol{\rho}\int d^2\boldsymbol{\rho}'\int d^2\boldsymbol{\eta}'[4\pi]^{-1}[\mathbf{i}\cdot\boldsymbol{\rho}][\boldsymbol{\eta}'\cdot\boldsymbol{\rho}]$$
$$\times[\pi\rho^4]^{-1}[\boldsymbol{\eta}'\cdot\boldsymbol{\rho}'][i\cdot\boldsymbol{\rho}'][\pi(\rho')^4]^{-1}\exp[-v_1\beta]. \tag{24a}$$

To assure that the sphere, whose surface generates $\eta'$, will not block the free path, the $\eta'$ integration in (24a) is over all orientations subject to the conditions

$$\eta'\cdot\rho \leqslant 0 \quad \text{and} \quad \eta'\cdot\rho' \geqslant 0. \tag{24b}$$

As the exclusion volume $v_1$ only depends on the two path displacement vectors $\rho$ and $\rho'$, the solid angle integration $d^2\eta'$, including the inequalities (24b), can be performed without an explicit form for $v_1$

$$\int d^2\eta'\rho\cdot\eta'\rho'\cdot\eta' = \tfrac{2}{3}\rho\rho'[\mu\arccos\mu-\sqrt{(1-\mu^2)}] \tag{25a}$$

where

$$\mu = \rho\cdot\rho'/(\rho\rho'). \tag{25b}$$

The overlap between the two cylinders and the two end spherical elements of the exclusion volume (Fig. 1(b)) can make $v_1$ geometrically complex, but the upper and lower limits,

$$\frac{4\pi a^3}{3}+\frac{\pi a^2\rho}{2}+\frac{\pi a^2\rho'}{2} \leqslant v_1 \leqslant \frac{4\pi a^3}{3}+\pi a^2\rho+\pi a^2\rho' \tag{26}$$

are always valid. The integrand of (24a) is positive, hence insertion of the upper or the lower limit (26) on $v_1$ into the exponential gives, respectively, lower or upper limits on the integral $G_1$.

$$I(\gamma) = 1-\phi+2\phi(3m\pi^3)^{-1}\int d^3\rho\int d^2\rho'[i\cdot\rho][i\cdot\rho']$$
$$\times[\rho\rho']^{-3}[\mu\arccos\mu-\sqrt{(1-\mu^2)}]\exp[\gamma(\rho+\rho')m^{-1}], \tag{27}$$

where $\mu$ is given by (25b)

$$I(1) \leqslant G_1 \leqslant I(1/2), \tag{28}$$

and $m$ is included from (19a) and (19c).

After integration over the cylindrical angular coordinate and the axial component of $\rho$ across the semi-infinite slab, and after several variable substitutions, we have

$$I(\gamma) = 1-\phi-\frac{4\phi}{3\gamma\pi^2}\int_0^1 dx\int_0^1 dy\frac{xy}{x+y}Q(x,y) \tag{29a}$$

$$Q(x,y) = \int_0^{2\pi} d\theta[\mu\arccos\mu-(1-\mu^2)^{1/2}] \tag{29b}$$

and

$$\mu = -xy+(1-x^2)^{1/2}(1-y^2)^{1/2}\sin\theta, \tag{29c}$$

where (19a) is used to eliminate $\sigma_s$ from the integral. The complete integrand of equation (29) is smooth and bounded. The double integral of (29a) and the single integral of (29b) are evaluated numerically using the composite, three-point Gaussian quadrature method,

$$\int_0^1 dx\int_0^1 dy\frac{xy}{x+y}Q(x,y) = -2.2934\ldots. \tag{30}$$

The resulting upper and lower limits from (28) for the integral $G_1$ are

$$1-0.6902\phi \leqslant G_1 \leqslant 1-0.3804\phi. \tag{31}$$

In turn from the truncated sum (11), the lower bound on the effective emissivity is

$$\varepsilon_{\text{eff}} \geqslant \varepsilon_s+0.3804\phi\varepsilon_s(1-\varepsilon_s) \tag{32}$$

and from (15) the complementary upper bound can be written either as

$$\varepsilon_{\text{eff}} \leqslant 1-(1-\varepsilon_s)(1-0.6902\phi) \tag{33a}$$

or

$$\varepsilon_{\text{eff}} \leqslant \varepsilon_s+0.6902\phi(1-\varepsilon_s). \tag{33b}$$

A major significance of $G_1$ is the introduction of an explicit void fraction dependence into the effective emissivity equations.

## RESULTS AND DISCUSSION

The two general summation forms are complementary in the sense, that the values (6) of $H_i$, $H_{i-1}$, ..., $H_0$ provides from (5), a lower bound on the effective emissivity, and the same set of integrals through (13) give an equivalent upper bound from (14). The integrals $H_i$ are independent of the surface properties of the solid and are determined only by the microstructure of the void–solid interface. $H_i$ can be evaluated from the structure without specifying the

particular solid material and $\varepsilon_{\text{eff}}$ determined once $\varepsilon_s$ is available. Two rigorous limits can be obtained from the full summation (5)

$$\lim_{\varepsilon_s \to 0} \varepsilon_{\text{eff}} = 0 \tag{34}$$

and with (10) for a semi-infinite slab

$$\lim_{\varepsilon_s \to 1} \varepsilon_{\text{eff}} = 1. \tag{35}$$

To our knowledge the relationship of $\varepsilon_{\text{eff}}$ to structural properties (e.g. the void fraction $\phi$ and average pore diameter $m$) for the important case of opaque, diffusely reflecting solid–void beds at various surface emissivities has not yet been systematically addressed in the previous theoretical [4, 5, 7, 8] or experimental efforts [3, 11]. In our calculations the average pore diameter appears in equation (27), but because the slab is semi-infinite it cancels out in (29) and (30) upon integration across the slab. For a finite thickness $L$, the pore diameter would enter in the dimensionless ratio $L/m$. In Fig. 2 the lower (32) and upper bounds (33) on the effective emissivity of a semi-infinite slab, cut from a bed of randomly overlapping spheres all of the same radius, provides useful information about the void fraction and surface emissivity dependence. For each surface emissivity value $\varepsilon_s$ shown in Fig. 2(a), the effective emissivity solid upper bound, dashed lower bound and dotted average mid point curve are straight lines with rather mild positive slopes, less than 0.7. The complementary upper and lower bounds converge in the limit $\phi \to 0$ to the solid surface emissivity, at zero porosity the porous material has the properties of the nonporous solid.

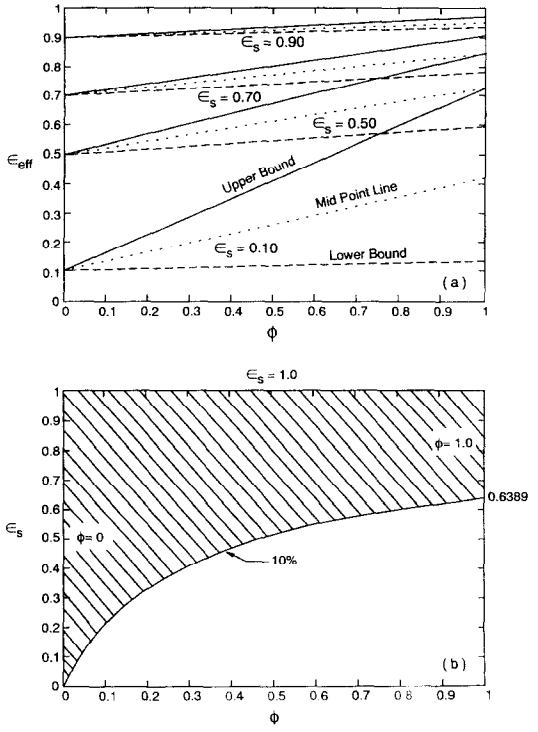


FIG. 2. (a) The effective emissivity upper bounds (——), (33), lower bounds (- - -), (32), and mid point estimates (···), (37), for a semi-infinite slab of randomly overlapping solid spheres all of the same radius vs the void fraction $\phi$ for various values of the void–solid interface emissivity $\varepsilon_s$; (b) maximum percent error bound, $100 \times \Delta\varepsilon_{\text{eff}}/\langle\varepsilon_{\text{eff}}\rangle_1$, vs surface emissivity $\varepsilon_s$ and void fraction $\phi$ for the estimate $\langle\varepsilon_{\text{eff}}\rangle_1$ of the effective emissivity of a semi-infinite slab cut from a bed of randomly overlapping spheres, $\langle\varepsilon_{\text{eff}}\rangle_1 = \varepsilon_s + (1-\varepsilon_s) \times (0.3451 + 0.1902\varepsilon_s)\phi$. The error (38) is less than 10% within the shaded region, and continuously decreases from 10% at the solid curve to zero along either line $\phi = 0$ or $\varepsilon_s = 1$.

A mechanistic explanation for the increase of the effective emissivity in Fig. 2(a) with the void fraction for $0 < \varepsilon_s < 1$ can be developed from the $\varepsilon_{\text{eff}}$ summation (5) and its path integrals (6). The first term in the sum contains the surface emissivity $\varepsilon_s$ and the wall to bed view factor $H_0$. As $H_0$ must be unity for a semi-infinite slab of any pore structure, the first term in the $\varepsilon_{\text{eff}}$ sum is $\varepsilon_s$. The second term includes the integral $H_1$, a sum of the differential view factors for all two segment radiation paths that begin with emission from the bed surface, followed by a single diffuse reflection and exit from the bed, multiplied by the emissivity factor $\varepsilon_s(1-\varepsilon_s)$. As the void fraction increases from zero, $H_1$ will start at zero and increase as the new bed void volume generates internal bed surface $\Sigma_{\text{int}}$ accessible to the outside edge $\Sigma_0$ (Fig. 1(a)) and corresponding new paths. Hence $\varepsilon_{\text{eff}}$ will increase with $\phi$. At higher void fractions, when a particle is removed at random, this opens paths so that radiation from deeper in the bed can exit, but as the slab is semi-infinite, there is no effective decrease in the internal surface area of the bed. Note that this may not be the case in an optically thin bed where decrease in surface area and deeper accessibility may increase the transmittance. The higher order terms of series (5) are all positive and the $H_i$ behave similarly to $H_1$. Both our results and those of Borodulya *et al.* [7, 8] show for intermediate surface emissivity values, the increase in $\varepsilon_{\text{eff}}$ with void fraction can be significant.

Note for each $\varepsilon_s$ value, the summations (5) and (14) also provide bounds on $\varepsilon_{\text{eff}}$ that do not depend on the bed microstructure, respectively, a lower bound $\varepsilon_s$ and upper bound 1. But these bounds are clearly not as good as those in Fig. 2(a). Grace used the mid point estimate from the 1, $\varepsilon_s$ bounds when he suggested the effective emissivity equation

$$\langle\varepsilon_{\text{eff}}\rangle_0 = 0.5(1+\varepsilon_s). \tag{36}$$

and compared it to a number of experimental data points in the *Handbook of Multiphase Systems* [11]. A mid point estimate based on the upper (33) and lower bounds (32) in Fig. 2(a), a systematic improvement on Grace's effective emissivity (36),

$$\langle\varepsilon_{\text{eff}}\rangle_1 = 0.5(1+\varepsilon_s) + 0.5(1-\varepsilon_s) \times (-1 + 0.6902\phi + 0.3803\phi\varepsilon_s) \tag{37}$$

is the analytical expression for the mid point dotted lines of Fig. 2(a). From the complementary upper and

lower bounds, we have in addition an error bound $\Delta\varepsilon_{\text{eff}}$,

$$\Delta\varepsilon_{\text{eff}} = (1-\varepsilon_s)(0.3451-0.1902\varepsilon_s)\phi. \quad (38)$$

The bounds (32) and (33) are always valid for a randomly overlapping sphere bed, however, for certain $\phi$ and $\varepsilon_s$ values, the estimate of the effective emissivity given by (37) is also useful. In Fig. 2(b) a maximum percent error bound $100\times\Delta\varepsilon_{\text{eff}}/\langle\varepsilon_{\text{eff}}\rangle_1$ for the estimate $\langle\varepsilon_{\text{eff}}\rangle_1$ from (37) and (38) is shown for various void fractions and surface emissivities. Within the shaded region the error is less than 10%. The error continuously decreases from 10% at the solid curve, across the shaded region, to zero along either edge $\phi = 0$ or $\varepsilon_s = 1$.

From the limit (35), the slope of the effective emissivity curve vs the void fraction should be zero for a black surface ($\varepsilon_s \to 1$), and this is the case for the bounds in Fig. 2(a) and the effective emissivity equation (37). That the slope of the void fraction dependence of the midpoint average dotted line in Fig. 2(a) and equation (37) initially increases with surface emissivity decreasing from unity, is also a reasonable result for a semi-infinite slab. With a surface emissivity less than one, and the additional surface reflections, an increasing void fraction will encourage emission contributions from surfaces deeper in the bed. But at some point the slope must turn around to achieve the zero slope predicted by the opposite limit (34) at perfect reflection ($\varepsilon_s \to 0$). Indeed the slope of the lower bound (32) reaches a maximum positive value of 0.0951 at $\varepsilon_s = 0.5$ and decreases back to zero at $\varepsilon_s = 0$. However, the slope of the upper bound (33) continues to increase to a maximum of 0.6902 at $\varepsilon_s = 0$. This weakness in the upper bound for $\varepsilon_s < 0.5$, and all but smaller values of $\phi$, is the most significant reason for the larger errors seen in the unshaded bottom region of Fig. 2(b).

Upper bounds (33) for $\phi = 0.4$, 0.70 and $\phi \to 1$; lower bounds (32) for $\phi = 0.4$ and $\phi \to 1$; the effective emissivity calculated from the two-flux model [4, 5], and the effective emissivity results for a cubic lattice of spheres obtained from the cell model approximation [7, 8] for $\phi \geqslant 0.95$ and $\phi = 0.4$ are all shown for comparison in Fig. 3(a). The cell model, cubic lattice dotted curve for $\phi = 0.4$ starts from the origin and crosses over the randomly overlapping sphere upper bound solid curve for $\phi = 0.4$ at $\varepsilon_s = 0.13$. From this $\varepsilon_s$ value on, the cubic lattice effective emissivity curve always lies above the random sphere bounds. The ordered structure of the cubic lattice gives a larger $\varepsilon_{\text{eff}}$ value due to the open channels that allow deeper radiation penetration. Effective emissivity values at lower void fractions will be sensitive to surface structure.

At higher void fractions in the random sphere bed, sphere overlap becomes unlikely and the randomly placed sphere model relates exactly to a gray gas or an idealized dilute fluidized bed of randomly placed solid spheres. The edge surface contribution also vanishes. Note that $G_1$ was split into an edge surface term and an internal surface term, $G_1^{\text{int}}$ for $\Sigma_{\text{int}}$ in (21). The edge term was shown to be $(1-\phi)$ and $G_1$ in (22) was written as their sum

$$G_1 = (1-\phi)+G_1^{\text{int}}. \quad (39)$$

The edge surface term, bracketed in (39), vanishes as $\phi \to 1$. However from (27)–(30), $G_1^{\text{int}}$ is bounded from above and below by a finite positive coefficient times $\phi$. Then $G_1^{\text{int}}$ (or at least its lower bound) must increase as $\phi \to 1$, and the cut sphere edge surfaces vanish from both $G_1$ and $\varepsilon_{\text{eff}}$ at higher void fraction. At higher void fractions our random sphere model is very similar to both the expanded cubic lattice for $\phi \geqslant 0.95$ and the two-flux sphere bed for $\phi \to 1$. Their effective emissivity curves are shown on Fig. 3(a) to lie between the high void fraction ($\phi \to 1$) upper (33) and lower (32) sum bounds for any value of the solid particle surface emissivity. Further in Fig. 3(a), both the expanded cubic lattice and two-flux effective emissivity curves cross the upper bound solid curve for $\phi = 0.7$, in fact the former touches the $\phi \to 1$ upper bound while the

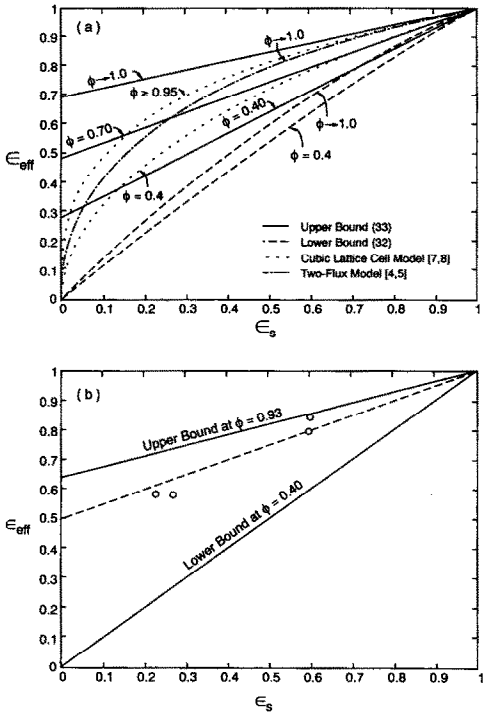


FIG. 3. (a) Effective emissivity upper bounds for a semi-infinite slab cut from a bed of randomly overlapping spheres (33) with $\phi = 0.4$, 0.7 and $\phi \to 1$; the corresponding lower bounds (32) with $\phi = 0.4$ and $\phi \to 1$; the effective emissivity calculated from the two-flux model; and the effective emissivity results for a cubic lattice of spheres obtained from the cell model approximation for $\phi \geqslant 0.95$ and $\phi = 0.4$ vs the surface emissivity $\varepsilon_s$; (b) measured fluidized bed effective emissivity values of unknown bed voidage from Grace [11] are compared with greatest upper (33) and least lower (32) bounds for a fluidized bed void fraction range (0.93–0.4). The dotted line is from an effective emissivity estimation $0.5\,(1+\varepsilon_s)$ suggested by Grace [11].

latter contacts the $\phi = 0.97$ upper bound. So they do not lie between the bounds (32) and (33) unless the void fraction is sufficiently high ($\phi \geqslant 0.97$). But this is consistent with the fact that the two-flux and expanded cubic lattice results in Fig. 3(a) are obtained for very dilute beds, and the truncated summation bounds (32) and (33) agree with the effective emissivity curves from these two well-known approximate methods.

In Fig. 3(b) some experimental values of the effective emissivity for a fluidized bed given by Grace [11] are compared with effective emissivity complementary bounds (32) and (33). While in each case the particle emissivity is known, no void fraction values were given. Using a possible range of void fraction (0.93–0.40) suggested by Borodulya and Kovensky [8] and putting aside any differences in structure at lower $\phi$ due to overlap, we can at least construct a greatest effective emissivity upper bound and smallest lower bound from these void fractions and see how well they do. Grace's [11] suggested effective emissivity estimate (36), which is also not dependent on structure, is included in Fig. 3(b). The data, though rather scattered, do lie within the predicted bounds.

## SUMMARY AND CONCLUSIONS

Two different infinite series in $(1-\varepsilon_s)^i$, (5) and (14), are presented for the effective emissivity of an arbitrary isothermal void–solid distribution, e.g. packed bed, fluidized bed or porous medium. Note that the isothermal condition is not necessarily restrictive because the differential volume element in the energy transport equations (which must be significantly larger than the microstructural scale) is usually assumed nearly isothermal in order that the transport coefficients can be evaluated at the local temperature. Besides $\varepsilon_s$, the coefficient of the $(1-\varepsilon_s)^i$ term in each sum depends on the same set of $i$ integrals $H_0$, $H_1, \ldots, H_i$ defined in (6). The integral $H_i$ counts those escape probabilities of an emitted photon with exactly $i$ surface reflections, and thus brings into $\varepsilon_{\text{eff}}$ the microstructure of the porous medium or random bed.

We demonstrate that it is not necessary to evaluate the series. Rigorous complementary upper and lower bounds on $\varepsilon_{\text{eff}}$, and often even a reasonable estimate with a built in error bound, can be generated after evaluating just the first few $i$ terms of each series. In principle the $H_i$ integrals can be evaluated in a number of different ways, direct simulation, Monte Carlo integration of the $H_i$ integrals or analytically as we have done here. That only the first few $i$ terms and hence the least complex paths are needed should shorten any of these approaches.

The method has been examined in the context of a model random void–solid distribution, a semi-infinite slab cut from a bed of randomly overlapping spheres. Results, which apply in general to a porous medium and for higher void fraction to a gray gas, fluidized bed, when compared to the two-flux and cell model calculations as well as experimental data, are within predicted limits.

## REFERENCES


1. A. Varma, G. Cao and M. Morbidelli, Self-propagating solid–solid noncatalytic reactions in finite pellets, *A.I.Ch.E. Jl* **36,** 1032–1038 (1990).
2. J. Szekely and J. W. Evans, A structural model for gas–solid reactions with a moving boundary—II. The effect of grain size, porosity and temperature on the reaction of porous pellets, *Chem. Engng Sci.* **26,** 1901–1913 (1971).
3. S. C. Saxena, K. K. Srivastava and R. Vadivel, Experimental techniques for the measurement of radiative and total heat transfer in gas fluidized beds: a review, *Exp. Thermal Fluid Sci.* **2,** 350–364 (1989).
4. M. Q. Brewster, Effective emissivity of a fluidized bed, HTD-40, ASME Winter Annual Meeting, New Orleans, Louisiana, pp. 7–13 (1984).
5. M. Q. Brewster, Effective absorptivity and emissivity of particulate media with application to a fluidized bed, *ASME J. Heat Transfer* **108,** 710–713 (1986).
6. C. L. Tien and B. L. Drolen, Thermal radiation in particulate media with dependent and independent scattering. In *Annual Review of Numerical Fluid Mechanics and Heat Transfer*, Vol. 1, pp. 1–32. Hemisphere, New York (1986).
7. V. A. Borodulya, V. I. Kovensky and K. E. Makhorm, Fluidized bed radiative heat transfer, *Proceedings of 4th International Conference on Fluidization* (Edited by D. Kunii and R. Toei), pp. 379–387. Engng Foundation, New York (1983).
8. V. A. Borodulya and V. I. Kovensky, Radiative heat transfer between a fluidized bed and a surface, *Int. J. Heat Mass Transfer* **26,** 277–287 (1983).
9. R. Siegel and J. R. Howell, *Thermal Radiation Heat Transfer*. McGraw-Hill, New York (1981).
10. D. Vortmeyer, Radiation in packed solids, *German Chem. Engng* **3,** 124–138 (1980).
11. J. R. Grace, Fluidized bed heat transfer. In *Handbook of Multiphase Systems* (Edited by G. Hestroni), pp. 8–72. Hemisphere, New York (1982).
12. J. J. Carberry, *Chemical and Catalytic Reaction Engineering*. McGraw-Hill, New York (1976).
13. N. Decker and L. R. Glicksman, Conduction heat transfer at the surface of bodies immersed in gas fluidized beds of spherical particles, *A.I.Ch.E. Symp. Series*, Vol. 77, No. 208, pp. 341–349 (1981).
14. N. Decker and L. R. Glicksman, Heat transfer in large particle fluidized beds, *Int. J. Heat Mass Transfer* **26,** 1307–1320 (1983).
15. W. Strieder and R. Aris, *Variational Methods Applied to Problems of Diffusion and Reaction*. Springer, Berlin (1973).